Atmospheric
Chemistry
and Physics

Source-explicit estimation of brown carbon in the polluted atmosphere over the North China Plain: implications for distribution, absorption, and the direct radiative effect

Jiamao Zhou[1,2], Jiarui Wu[1], Xiaoli Su[1], Ruonan Wang[1], Imad EI Haddad[4], Xia Li[1], Qian Jiang[1], Ting Zhang[1], Wenting Dai[1], Junji Cao[3], Andre S. H. Prevot[4], Xuexi Tie[1], and Guohui Li[1]

[1]State Key Laboratory of Loess Science, Institute of Earth Environment, Chinese Academy of Sciences, Xi'an 710061, China
[2]National Observation and Research Station of Regional Ecological Environment Change and Comprehensive Management in the Guanzhong Plain, Xi'an 710061, China
[3]Institute of Atmospheric Physics, Chinese Academy of Sciences, Beijing 100029, China
[4]PSI Center for Energy and Environmental Sciences, Paul Scherrer Institute, 5232 Villigen, Switzerland

Correspondence: Guohui Li (ligh@ieecas.cn)

Abstract. Brown carbon (BrC) plays a significant role in altering atmospheric radiation. Beyond biomass and biofuel combustion, recent studies identify fossil fuel sources – especially residential coal burning and vehicle exhaust – as major contributors to BrC. This underscores a gap in climate models, which often assume fossil fuel organic aerosols (OAs) are non-absorbing or treat all OA as light-scattering. In this study, we simulate BrC over the North China Plain (NCP) during a winter pollution event using the WRF-Chem model, incorporating explicit BrC absorption properties. The model aligns well with observed pollutant and aerosol levels, revealing an average near-surface BrC concentration of $5.2\,\mu\mathrm{g\,m^{-3}}$, contributing $16.4\,\%$ to aerosol absorption at $365\,\mathrm{nm}$. Using a diagnostic adjoint approach, we estimate that BrC exerts a direct radiative effect (DRE) averaging $-0.09\,\mathrm{W\,m^{-2}}$ at the top of the atmosphere, reducing the cooling effect of organic carbon by $28.0\,\%$ and producing a local warming effect of up to $+0.40\,\mathrm{W\,m^{-2}}$. Coal combustion is the largest BrC source in the NCP in 2014, though secondary BrC also significantly impacts the regional radiation balance.

1 Introduction

Brown carbon (BrC) is a collective component for those colored organic compounds with wavelength-dependent light absorption properties (Mukai and Ambe, 1986; Kirchstetter et al., 2004; Andreae and Gelencsér, 2006). BrC has been recognized as an important short-lived climate forcer contributing considerably to climate change by warming of the atmosphere (IPCC, 2013; Feng et al., 2013; Jacobson, 2014; Jo et al., 2016; Brown et al., 2018). A study suggested that the light absorption induced by BrC can be equal to or even higher than that of black carbon (Pokhrel et al., 2017) and

substantially influences atmospheric radiative forcing. Recent studies have shown that BrC accounts for 30 %–50 % of the total absorption of aerosols in Atlanta, USA; Brazil; and Hebei, China (Hoffer et al., 2006; Yang et al., 2009; Liu et al., 2013). The direct radiation effect (DRE) caused by BrC is greater than $+1\,\mathrm{W\,m^{-2}}$ in some regions, such as South Asia, Africa and Southeast Asia, much higher than the global average (Park et al., 2010; Feng et al., 2013; Lin et al., 2014; Saleh et al., 2014; Jo et al., 2016; Wang et al., 2018; Yan et al., 2018). However, the modeled DRE associated with BrC remains highly uncertain, with variations spanning an order of magnitude difference. In particular, the

estimated global DRE of BrC is in the range between $+0.03$ and $+0.57\,\mathrm{W\,m^{-2}}$ (Hammer et al., 2016), which is caused by the limited observations of BrC mass and absorption properties (Tuccella et al., 2020; Saleh, 2020).

It has been well established that BrC is not a single substance but a general term for light-absorbing organic aerosols. A series of laboratory measurements and observations in the earlier years demonstrate that BrC is mainly associated with smoldering biomass burning (BB) or biofuel (BF) combustion (Chakrabarty et al., 2010; Chen and Bond, 2010; Lack et al., 2012; Washenfelder et al., 2015; Kumar et al., 2018). On the other hand, OAs from fossil fuel combustion are generally assumed to be non-absorbing as the combustion conditions for fossil fuels (FFs) are typically not conducive to BrC formation (Hecobian et al., 2010; Shapiro et al., 2009; Bond et al., 2013). Therefore, earlier climate model studies have assumed that primary OA from BB and BF combustion is the main or sole BrC source (Feng et al., 2013; Jacobson, 2014; Saleh et al., 2014; Hammer et al., 2016; Brown et al., 2018). Recent studies have also incorporated the aging of secondary organic aerosol (SOA) (Jo et al., 2016; Wang et al., 2018; Zhang et al., 2020). However, more recent exceptions are being found in low-efficiency residential coal combustion (RCC) (Bond, 2001; Yan et al., 2017; Xie et al., 2019; Tian et al., 2019; Zhang et al., 2022a) and fuel oil combustion in vehicle and ship engines (Xie et al., 2017; Corbin et al., 2019; Tang et al., 2020; Huang et al., 2022). It is now generally accepted that the formation of BrC is not exclusively linked to the chemical make-up of biomass fuels but is most critically determined by the combustion conditions (Saleh et al., 2018; Cheng et al., 2020; Saleh, 2020; Wang et al., 2022a). The key factor contributing to the high levels of BrC observed from biomass fuels is their combustion under relatively low-temperature and fuel-rich conditions, which are highly favorable for BrC formation. In contrast, fossil fuels, such as those burned in internal combustion engines, typically undergo combustion at higher temperatures and under more fuel-lean conditions, which are less conducive to BrC production (Saleh, 2020). In China, a developing country, coal is commonly used for residential heating in the cold season, causing massive emissions of organic particles (Yan et al., 2017; Li et al., 2018). According to the National Bureau of Statistics of China (https://data.stats.gov.cn, last access: 10 March 2025), the coal consumption in 2014 was about 4000 Tg, accounting for 65.8 % of the total primary energy use of China. Of this, around 93 Tg is used as household fuel. The poor burning conditions and limited emission control facilities in this region could lead to substantial emissions of BrC. This could explain why, to date, all reported instances of coal-derived BrC have originated from China. Both Yan et al. (2017) and Mo et al. (2021) used dual carbon isotope-based source apportionment methods and reported that fossil fuel, especially coal combustion from the residential sector, is an important source in northern China and even the largest contributor in some regions.

These recent findings indicate a critical gap in the treatment of BrC in chemical transport models, atmospheric chemistry models and climate models as well, which present an even greater concern, as they typically do not consider BrC at all (Ma et al., 2021; Jo et al., 2023; Gao et al., 2025; Ge et al., 2025). Addressing this gap requires expanding the scope of BrC sources and assigning distinct optical properties for each source and incorporating those that have been underrepresented or overlooked in past assessments into numerical models. In this study, we include the main primary emission sources (RCC, BB, BF and FF emissions from RCC and on-road vehicles (FF-TRA)) of BrC and secondary-derived BrC in a regional model, the Weather Research and Forecasting model coupled with Chemistry (WRF-Chem). A representative region, the North China Plain (NCP), is chosen as the study domain with high anthropogenic carbonaceous aerosols due to the widespread use of coal and biomass burning for heating during winter and the increasing number of motor vehicles. We performed a month-long simulation to evaluate the surface distribution, absorption and the DRE of BrC in the NCP, by updating BrC optical properties of different sources. Sensitivity experiments have also been devised to assess the contribution of BrC from major sources.

2 Model and method

2.1 WRF-Chem model and configurations

The WRF-Chem model (Grell et al., 2005; Fast et al., 2006) modified by Li et al. (2010, 2011a, b, 2012) is used to quantitatively estimate the BrC in the NCP. A heavily polluted month from 1 to 30 January 2014 is selected for the simulation period. The anthropogenic emissions are developed by Zhang et al. (2009) and Li et al. (2017), including five sources, namely agriculture, industry, power generation, residential, and transportation. The biogenic emissions are calculated online using the MEGAN (Model of Emissions of Gases and Aerosol from Nature) model developed by Guenther et al. (2006). Additionally, the grid-based RCC, BB and BF combustion emissions are used to update the BrC sources in this study, described later. The model simulation domain is shown in Fig. 1. The detailed model description and configurations can be found in Sect. S1 and Table S1 in the Supplement, respectively.

2.2 Aerosol radiative module

The aerosol radiative module developed by Li et al. (2011a) has been incorporated into the WRF-Chem model to calculate the aerosol optical depth (AOD or τ_a), single scattering albedo (SSA or ω_a), and asymmetry factor (g_a). In the aerosol module, aerosols are represented by a three-moment
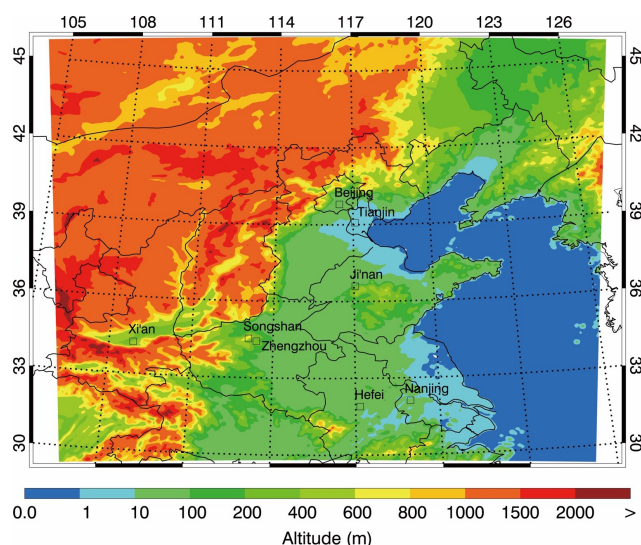
Figure 1. WRF-Chem simulation domain with topography. The square denotes the field sites for simulation and observation comparison.

approach with a lognormal size distribution:

$$n(\ln D) = \frac{N}{\sqrt{2\pi}\ln\sigma_g}\exp\left[-\frac{1}{2}\left(\frac{\ln D - \ln D_g}{\ln\sigma_g}\right)^2\right], \qquad (1)$$

where D is the particle diameter, N is the number distribution of all particles in the distribution, D_g is the geometric mean diameter, and σ_g is the geometric standard deviation. To calculate the aerosol optical properties, the aerosol spectrum is divided into 48 bins from 0.002 to 20.0 μm, with radius r_i. The aerosols are classified into four types: (1) internally mixed sulfate, nitrate, ammonium, hydrophilic organics and black carbon (BC) and water; (2) hydrophobic organics; (3) hydrophobic BC; and (4) other unidentified aerosols (generally dust-like aerosols). These four kinds of aerosols are assumed to be mixed externally. For the internally mixed aerosols, the complex refractive index at a specific wavelength (λ) is calculated based on the volume-weighted average of the individual refractive index. Given the particle size and complex refractive index and the extinction efficiency (Q_e), ω_a and g_a are calculated using the Mie theory at a certain wavelength (λ). The look-up tables of Q_e, ω_a and g_a are established according to particle sizes and refractive indices to avoid multiple Mie scattering calculation. The aerosol optical parameters are interpolated linearly from the look-up tables with the calculated refractive index and particle size in the module. The τ_a at a certain λ in a given atmospheric layer k is determined by the summation over all types of aerosols and all bins:

$$\tau_a(\lambda k) = \sum_{i=1}^{48}\sum_j^4 Q_e(\lambda, r_i, j, k)\pi r_i^2 n(r_i, j, k)\Delta Z_k, \qquad (2)$$

where $n(r_i, j, k)$ is the number concentration of the jth kind of aerosols in the ith bin. ΔZ_k is the depth of an atmospheric layer. The weighted-mean values of ω_a and g_a are then calculated using D'Almeida et al. (1991):

$$\omega_a(\lambda, k) = \frac{\sum_{i=1}^{48}\sum_j^4 Q_e(\lambda, r_i, j, k)\pi r_i^2 n(r_i, j, k) \times \omega_a(\lambda, r_i, j, k)\Delta Z_k}{\sum_{i=1}^{48}\sum_j^4 Q_e(\lambda, r_i, j, k)\pi r_i^2 \times n(r_i, j, k)\Delta Z_k} \qquad (3)$$

$$g_a(\lambda, k) = \frac{\sum_{i=1}^{48}\sum_j^4 Q_e(\lambda, r_i, j, k)\pi r_i^2 n(r_i, j, k) \times \omega_a(\lambda, r_i, j, k)g_a(\lambda, r_i, j, k)\Delta Z_k}{\sum_{i=1}^{48}\sum_j^4 Q_e(\lambda, r_i, j, k)\pi r_i^2 n(r_i, j, k) \times \omega_a(r_i, j, k)\Delta Z_k}. \qquad (4)$$

When the wavelength-dependent τ_a, ω_a, and g_a are calculated, they can be used in the Goddard shortwave module.

It is worth noting that the aerosol liquid water content in the study is predicted with the inorganic aerosols using a computationally efficient thermodynamic equilibrium model, ISORROPIA (version 1.7, Nenes et al., 1998; Fountoukis and Nenes, 2007). In this study, ISORROPIA is mainly used to predict the thermodynamic equilibrium between the ammonium–sulfate–nitrate–chloride–water aerosols and their gas-phase precursors H_2SO_4–HNO_3–NH_3–HCL–water vapor, and water uptake of aerosols is calculated using the Zdanovskii–Stokes–Robinson (ZSR) correlation (Stokes and Robinson, 1966):

$$W = \sum_i \frac{M_i}{m_{oi}(a_w)}, \qquad (5)$$

where W is the mass concentration of aerosol liquid water (kg m^{-3} air), M_i is the molar concentration of species i (mol m^{-3} air) and $m_{oi}(a_w)$ is the molality of an aqueous binary solution of the ith electrolyte with the same a_w (i.e. relative humidity) as in the multicomponent solution.

The BrC in the model has an effective density of 1.2 g cm^{-3} for primary BrC (Turpin and Lim, 2001) and of 1.0 g cm^{-3} for secondary BrC (Hurley et al., 2001). The imaginary refractive index of BrC used in this study is discussed in Sect. 2.3.2.

2.3 Model modifications

2.3.1 Source separation of BrC

The definition of BrC in the model is dependent on its sources. Due to the lack of BrC emission inventories, according to the characteristics of energy structure in China, assumptions and code modifications of the WRF-Chem model have been made to consider the BrC from different sources. These involve three separate primary BrC sources, including BB emissions, FF emissions from RCC and on-road vehicles (FF–TRA), and SOA with light-absorbing properties, whereas other types of primary OA (POA) and SOA are assumed to be purely scattering. In this study, the BB source corresponds to open fire, household biomass burning and biofuel consumption emissions.

For the primary emissions, previous BrC simulations have substituted it with a proportion of POA directly (Feng et al., 2013; Lin et al., 2014; Wang et al., 2014; Tuccella et al., 2020; Xu et al., 2024), derived it from the relationship between the burning efficiency and the observed aerosol light absorption (Jo et al., 2016; Zhu et al., 2021), or determined it through parameterization where BrC absorption is a function of the BC-to-OA emission ratio (Zhang et al., 2020). In the present work, we calculated the primary BrC emissions based on the bottom-up OA emission inventory combined with reported annual BrC emissions from various primary sources, as shown in Table 1. Firstly, we collected the reported annual emissions of BrC from RCC, BB and FF-TRA by using bottom-up inventory method. It should be noted that given the proximity of the study period (January 2014) to 2013, we use the emissions of BrC from RCC and BB in 2013 provided by Sun et al. (2017, 2021), which is 592 and 712 Gg, respectively. The emissions of FF-TRA-derived BrC are 76 Gg, which is calculated based on the value of 2017 (Wang et al., 2022a) and scaled by a factor of 0.70 to reflect the change of annual civilian-owned motor vehicles. We assume that the spatial and seasonal variation of BrC is similar to OA. Then, the monthly BrC emissions from the bottom-up emissions inventory in the NCP in January 2014 are the annual BrC emissions multiplied by the ratio of OA emissions in the NCP vs China and the ratio of OA emissions in January 2014 vs the whole year, resulting in a value of 65.5, 56.8 and 4.4 Gg for RCC, BB and FF-TRA, respectively. Finally, the proportion of the three primary types of emissions of BrC used in the model is 36.3 %, 100.8 % and 15.8 %, respectively. Figure 2 shows the contributing regions and burdens of the three separate primary sources of BrC.

SOA has also shown light absorption in the atmosphere (Lin et al., 2014). Laboratory experiments have revealed that most of the light-absorbing SOA is associated with aromatic SOA (Jacobson, 1999; Laskin et al., 2015; Li et al., 2020), and the absorption from biogenic SOA in the field has been found to be negligible (Washenfelder et al., 2015). Therefore, here we assume aromatic-derived SOA as secondary BrC in the model following previous studies (Jo et al., 2016; Wang et al., 2018).

Moreover, it is worth noting that both POA light absorption and SOA light absorption were shown to be dynamic, where BrC can be bleached when they undergo photodissociation (Forrister et al., 2015; Wong et al., 2019) or be darkened by cloud and fog processing of aerosols (Moise et al., 2015; Lin et al., 2017; Cheng et al., 2020). These processes are not considered in this study yet. More detailed parameterization of the chemical aging of BrC is needed in future BrC models.

2.3.2   BrC optical properties

The refractive indices of BrC as a function of wavelength are used for radiative transfer calculations. The complex refractive index ($m = n + ik$) of aerosol components enables practical implementation in the model, where n is the real part primarily associated with the scattering efficiency, and k is the imaginary part primarily associated with the absorption efficiency (Bohren and Huffman, 1998). The real part of BrC refractive index is the same of non-absorbing OA, which is fairly constrained, with reported values typically ranging from 1.5 to 1.7 (Saleh et al., 2014; Browne et al., 2019; Li et al., 2020). This study follows the study by Li et al. (2011a) and Wu et al. (2020). The imaginary part (k) of the BrC refractive index exhibits strong wavelength dependence, and the values range over several orders of magnitude (Saleh et al., 2018; Sengupta et al., 2018). Limited studies on the optical properties of BrC from fossil fuel combustions are reported at present. The average mass absorption efficiency (MAE) of RCC at 365 nm ranges from 0.80 to 2.47 m^2 g^{-1} (Yan et al., 2017; Li et al., 2019; Tang et al., 2020; Wang et al., 2020; Ni et al., 2021; Song et al., 2021; Wang et al., 2021). In this study, as shown in Table 2, two sets of MAE are used for the sensitivity experiments of BrC. We choose a field optical measurement of BrC from all sources made by Zhang et al. (2022b) as the high absorption case (HI-BRC-ABS). The optical properties of BB and FF-TRA obtained in laboratory by Xie et al. (2017), as well as MAE of RCC and secondary BrC obtained in laboratory by Ni et al. (2021), are adopted as the low absorption case (LOW-BRC-ABS) in the study. The imaginary part of the two cases has shown wavelength-dependent light absorption properties and that the changes in anthropogenic emissions affect the optical properties of BrC. The imaginary part of both two cases is interpolated to 11 wavelengths to match the aerosol radiation calculation of the Goddard module in WRF-Chem. The value of k in this work is derived from the measured MAE using the following equation (Liu et al., 2013; Lu et al., 2015), as shown in Table 2:

$$k_{\mathrm{BrC},\,\lambda} = \frac{\rho \times \lambda \times \mathrm{MAE}_\lambda}{4\pi}, \tag{6}$$

where MAE_λ (m^2 g^{-1}) is the bulk mass absorption efficiency of BrC at the corresponding wavelength λ. ρ (g cm^{-3}) is the density of organic aerosols, which is calculated to be 1.2 g cm^{-3} (Turpin and Lim, 2001) in this study.

2.3.3   Shortwave direct radiative effect calculation and experimental design

The shortwave DRE calculations of BrC follow the method reported by Chen et al. (2021) as shown in Eq. (7). The DRE of BrC is calculated by the difference between the net radiant flux with and without BrC, where the net radiant flux is the difference between the downward ($F_\downarrow$) and upward radiant flux ($F_\uparrow$).

$$\mathrm{DRE_{TOA}} = \left(F^{\mathrm{a}}_{\downarrow\mathrm{TOA}} - F^{\mathrm{a}}_{\uparrow\mathrm{TOA}} \right) - \left(F^{0}_{\downarrow\mathrm{TOA}} - F^{0}_{\uparrow\mathrm{TOA}} \right), \tag{7}$$

Table 1. The data for primary BrC emissions calculation.

Primary sources of BrC	RCC	BB	FF-TRA
Annual BrC emissions (Gg) in China	592.0[a]	712.0[b]	76.0[c]
Ratio of OA emissions in the NCP vs China[e]	57.7 %	51.0 %	69.4 %
Ratio of OA emissions in January 2014 vs the whole year[e]	19.2 %	14.0 %	8.3 %
Bottom-up emissions inventory induced monthly BrC emissions in the NCP in January	65.5	56.8[d]	4.4
Emissions in the NCP in January 2014[e]	180.2	56.4	27.9
BrC emissions ratio for primary sources used in the model	36.3 %	100.8 %	15.8 %

[a] The BrC emissions from China's RCC in 2013 were reported by Sun et al. (2017) based on experiments involving seven types of coal being burned in four typical stoves in both chunk and briquette style. [b] The calculated BrC emissions from China's household biomass burning in 2013 were reported by Sun et al. (2021) using 11 widely used biomass types in China burned in a typical stove. [c] The estimated BrC emissions from vehicle exhaust in 2017 were 109 Gg reported by Wang et al. (2022a). In this study, the emissions of FF-TRA-derived BrC is 76.0 Gg, with a yearly scale factor of 0.70, which is derived by the annual level of civilian-owned motor vehicles between 2014 and 2017. [d] The value of BrC emissions in the NCP in January 2014 is additionally added with OA emitted from open biomass burning (6 Gg), which is assumed to be entirely light-absorbing. [e] These values were derived from the OA emission inventory described in Sect. 2.1.
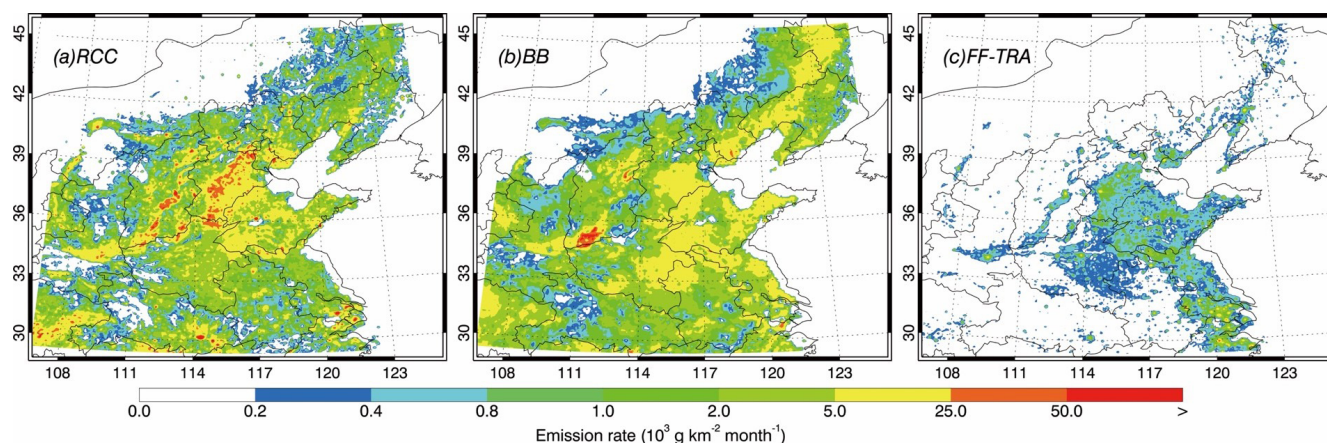
Figure 2. Monthly BrC emissions burdens in January 2014 in the NCP from RCC, BB and FF-TRA.

where DRE_{TOA} represent the shortwave DRE at the top of the atmosphere (TOA). F^a and F^0 are the radiant flux with and without BrC aerosols, respectively.

An adjoint methodology proposed by Zhao et al. (2013) and Huang et al. (2015) has been used to diagnose the optical depth and DRE of BrC aerosols. Optical properties and radiative transfer of different sources BrC are calculated multiple times with one or a group of aerosol mass removed or without BrC absorption from each calculation following Eqs. (8) and (9). In addition, the model also takes into account the reduced aerosol masses along with the change in aerosol number concentration and size distribution.

$$AOD_{[species\,i]} = AOD_{[all\,species]}$$
$$- AOD_{[without\,species\,i\,/\,without\,species\,i\,absorption]} \quad (8)$$
$$DRE\;Forcing_{[species\,i]} = DRE\;Forcing_{[all\,species]}$$
$$- DRE\;Forcing_{[without\,species\,i\,/\,without\,species\,i\,absorption]} \quad (9)$$

This method is more efficient than the traditional approach of running the model multiple times with the exclusion of a specific aerosol component. It not only saves computational time but also provides a more accurate estimation focused solely on the direct radiative effect of aerosols.

Table 2. The refractive index of BrC used in the model.

Aerosols	Wavelength (nm)	k values for HI-BRC-ABS	k values for LOW-BRC-ABS
BrC-RCC	365	–	0.0320
	370	0.1890	–
	470	0.0608	–
	500	–	0.0020
	520	0.0272	–
	590	0.0173	–
	660	0.0081	–
BrC-BB	365	–	0.0300
	370	0.0587	–
	405	–	0.0016
	470	0.0219	–
	520	0.0120	–
	550	–	0.0026
	590	0.0092	–
	660	0.0046	–
BrC-FF-TRA	365	–	0.0180
	370	0.0509	–
	405	–	0.0130
	470	0.0194	–
	520	0.0085	–
	550	–	0.0045
	590	0.0046	–
	660	0.0018	–
BrC-SOA	365	–	0.0049
	370	0.0251	–
	470	0.0166	–
	500	–	0.0007
	520	0.0114	–
	590	0.0107	–
	660	0.0063	–

"–" means not available.

3　Results and discussions

3.1　Model performance

Before evaluating the DRE of BrC, results from the standard simulation are used to validate the model performance. Using available measurements, we first validate the spatial distribution and temporal variation of air pollutants ($PM_{2.5}$, O_3, NO_2, SO_2) in the NCP; the temporal variation of downward shortwave flux at the surface (SWDOWN) in Beijing, Tianjin, Zhengzhou, Hefei and Ji'nan; and the temporal variation of aerosol species (OA, elemental carbon, ammonium, sulfate and nitrite) in Beijing and Tianjin and of primary OA from BB, RCC, motor vehicles and SOA in Beijing in January 2014. Detailed data descriptions and quantitative statements of model biases can be found in Supplement Sects. S2.1 and S3. In general, the model simulates the air pollutants, SWDOWN, and aerosol species against measurements reasonably well.

SSA determines the strength of aerosols in absorbing solar radiation. Here we conduct three sensitivity experiments to evaluate the effect of BrC with different k values on the simulated aerosol absorption. The first experiment is the control simulation in which all organic aerosols are treated as purely scattering particles with no absorption contribution of BrC, which is referred to as NOBRC. The high-absorption scenario (HI-BRC-ABS) and low-absorption scenario (LOW-BRC-ABS) characterize BrC light absorption using the higher and lower imaginary refractive index derived from Sect. 2.3.2, respectively. Figure 3 shows the comparisons of simulated versus observed SSA at 440 nm (SSA_{440}) at Sun-sky radiometer Observation NETwork (SONET) sites in Beijing, Songshan, Xi'an, Hefei and Nanjing in January 2014. Due to the influence of clouds, the observational data from SONET are not continuous, resulting in a total of 237 valid data points being available for comparison. Moreover, SSA retrieval typically has larger uncertainties at low AOD values (Dubovik et al., 2002). Therefore, we have ex-
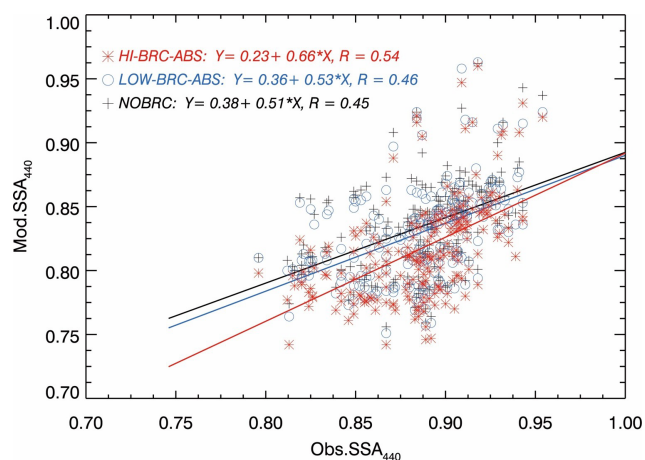
Figure 3. Scatter plot and linear fitting of modeled and observed column integrated SSA at 440 nm in case HI-BRC-ABS (red), LOW-BRC-ABS (blue) and NOBRC (black) case.

cluded the SSA data when AOD is less than 0.5, which leaves 206 valid points in each case. We find that the inclusion of BrC in the model reduces the bias of simulated SSA. The HI-BRC-ABS case demonstrated the largest improvement, with the correlation coefficient increasing to 0.54, making it the best simulation in the study. This suggests that the stronger BrC absorption case, as prescribed in HI-BRC-ABS, better captures the aerosol optical properties observed in northern China during winter. Consequently, the HI-BRC-ABS case can serve as the base simulation for further investigation of radiative effects of BrC in this study. Overall, the model tends to underestimate SSA_{440}. The underestimation might be partly caused by the overestimation of absorbing aerosols like BC or dust. Meanwhile, the uncertainties of the simulated SSA can be caused by other factors, such as mixing state of aerosols, particle shape, wavelength, and mass ratio of non-black carbon to BC (Liu et al., 2017; Jeong et al., 2020).

The daily AOD at 550 nm (AOD_{550}) from the dataset of Long-term Gap-free High-resolution Air Pollutant (LGHAP), derived via tensor-flow-based multimodal data fusion method (Bai et al., 2022), is compared with the simulation. This gap-free daily AOD dataset at 1 km resolution for 2000–2020 in China was generated by integrating multimodal data from satellites, numerical models, and in situ measurements. Data gaps in Moderate Resolution Imaging Spectroradiometer (MODIS) AOD are reconstructed through spatial pattern recognition and statistical knowledge transfer. Validation against Aerosol Robotic Network (AERONET) observations showed strong agreement, with an R of 0.91 and an RMSE of 0.21. Figure 4a and b show the pattern comparison of the monthly simulated and retrieved AOD_{550}. The model reproduces the retrieved AOD distribution in the NCP reasonably. The monthly average simulated and retrieved AOD_{550} is 0.45 and 0.48 on average in the NCP, respectively.
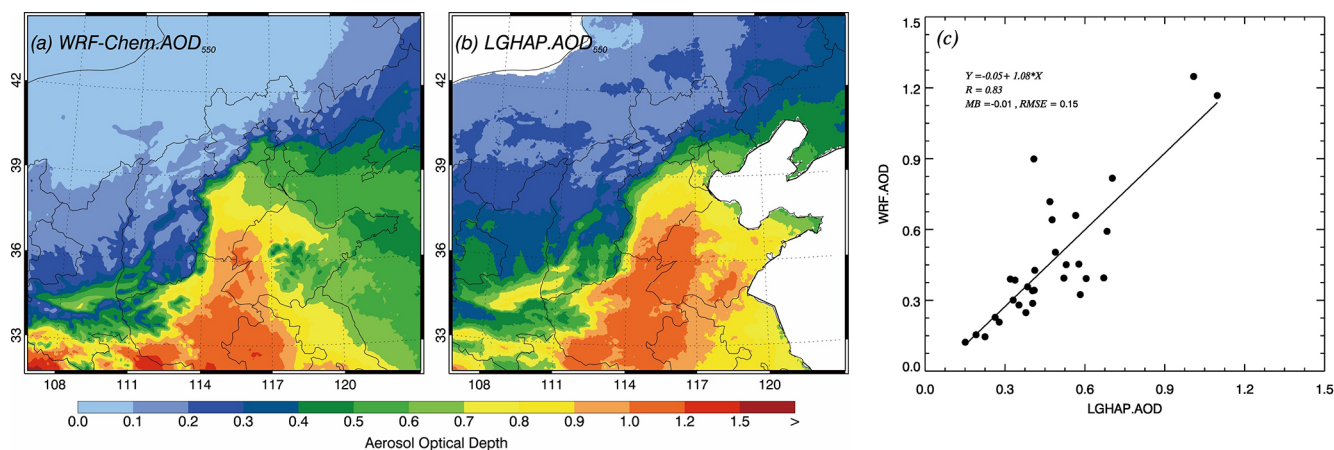
Figure 3c shows the scatter plot of the daily simulated and retrieved AOD_{550} averaged in the NCP during the simulation period. The simulated daily average AOD_{550} correlates quite well with the retrieved value, with a regression slope of 1.08 and correlation coefficient of 0.83. Generally, the retrieved and simulated AOD increases with deterioration of the particulate pollution. Figure 5 provides the pattern comparison of the simulated and Ozone Monitoring Instrument (OMI) retrieved AOD at 440 nm (AOD_{440}) averaged during the simulated episode. OMI aboard NASA's Aura satellite offers global atmospheric measurements at a spatial resolution of $0.25° × 0.25°$, with Beijing's overpass occurring at approximately 13:45 local time. The averaged AOD_{440} from the model simulation at 14:00 local time shows generally agreement with the OMI retrieval. The average simulated and retrieved AOD_{440} is 0.51 and 0.53 in the NCP, respectively. Overall, the model generally performs well in simulating the AOD distribution. It is worth noting that the simulated AOD is not only dependent on the column aerosol content and composition but is also substantially influenced by relative humidity (RH), which determines the aerosol hygroscopic growth. Additionally, the satellite-retrieved AOD is subject to contamination by the presence of clouds, and considering the high occurrence frequency of clouds during haze days, the retrieved AOD might be overestimated (Satheesh et al., 2010; Chand et al., 2012).

## 3.2 Surface mass concentrations of BrC in the NCP

The simulated distribution of average near-surface BrC concentrations and each source contribution in January 2014 is shown in Fig. 6a. In January, the monthly mean concentrations of BrC in the NCP vary from 0.05 to 42.3 µg m^{-3}, with an average of 5.2 µg m^{-3}. The spatial distribution of near-surface BrC concentrations is like that of PM$_{2.5}$ in the NCP, with the highest concentration areas located in Hebei Province, with an average concentration of 14.9 µg m^{-3}. The simulated BrC concentrations are higher than those reported by Zhu et al. (2021) in 2018, which is perhaps caused by the more severe particulate pollution in January 2014.

Figure 6b–e present the average near-surface BrC concentrations from different anthropogenic sources and secondary formation in January 2014 in the NCP. The BrC in the NCP predominantly originates from RCC and BB, with an average contribution of 2.3 and 2.4 µg m^{-3} and a maximum of 33.8 and 31.6 µg m^{-3}, respectively. A relatively small proportion of BrC is related to FF-TRA and secondary transformations with an average concentration of 0.2 and 0.4 µg m^{-3}, respectively. The BrC from RCC accounts for 55.8 % of total BrC concentrations in the NCP, which is highest in Beijing, Hebei and Tianjin, reaching 67.7 %, 54.4 % and 53.3 %, respectively. The BrC from BB constitutes 36.9 % of total BrC concentrations, with a contribution of about 40 % in most provinces of the NCP but only 26.5 % in Beijing. This result shows that the RCC is one of the major sources of BrC in

Figure 4. (a) Monthly simulated AOD_{550} of WRF-Chem, **(b)** monthly retrieved AOD_{550} of reanalysis dataset LGHAP, and **(c)** scatter plot of the daily simulated and retrieved AOD_{550} averaged in the NCP from 1 to 30 January 2014.
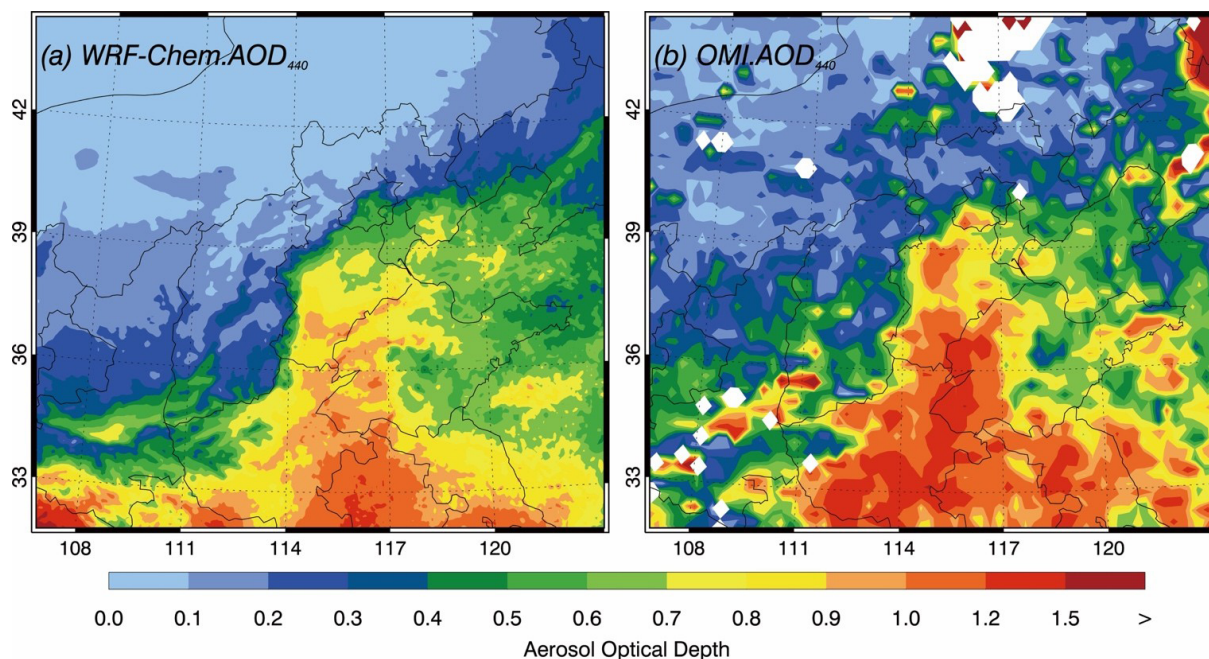

Figure 5. (a) Monthly simulated AOD_{440} of WRF-Chem and **(b)** monthly retrieved AOD_{440} of OMI in the NCP from 1 to 30 January 2014.

the NCP due to the wide use of coal for heating and cooking in winter with low combustion efficiency and little emission control. The BrC emitted by RCC is mainly concentrated in the Beijing–Tianjin–Hebei (BTH) region in January 2014, while the BrC emitted by BB is distributed in the whole NCP. The Fen-Wei Plain exhibits notably high contributions from BB, which is consistent with the emission distribution and with previous studies (Cao and Cui, 2021; Zhang et al., 2021). The Fen-Wei Plain is one of the most densely populated and heavily polluted areas in northern China where biomass is usually used for heating during winter.

3.3 BrC absorption in the NCP

BrC absorbs visible to near-ultraviolet light with its absorption capabilities extending prominently at shorter wavelengths. Therefore, we calculate the AAOD (aerosol absorption optical depth) to evaluate the absorption contribution of BrC versus bulk aerosols, each anthropogenic source and SOA versus BrC at 365 nm (Fig. 7), by differentiating the AAOD between the model runs with and without the contribution of BrC. The average contribution of BrC to the total AAOD of aerosols at 365 nm is 16.4 %, and the maximum is 39.5 % in the NCP in January 2014. The BrC to BC and OC ratios in surface air in the study is 2.2 and 0.31, respectively.
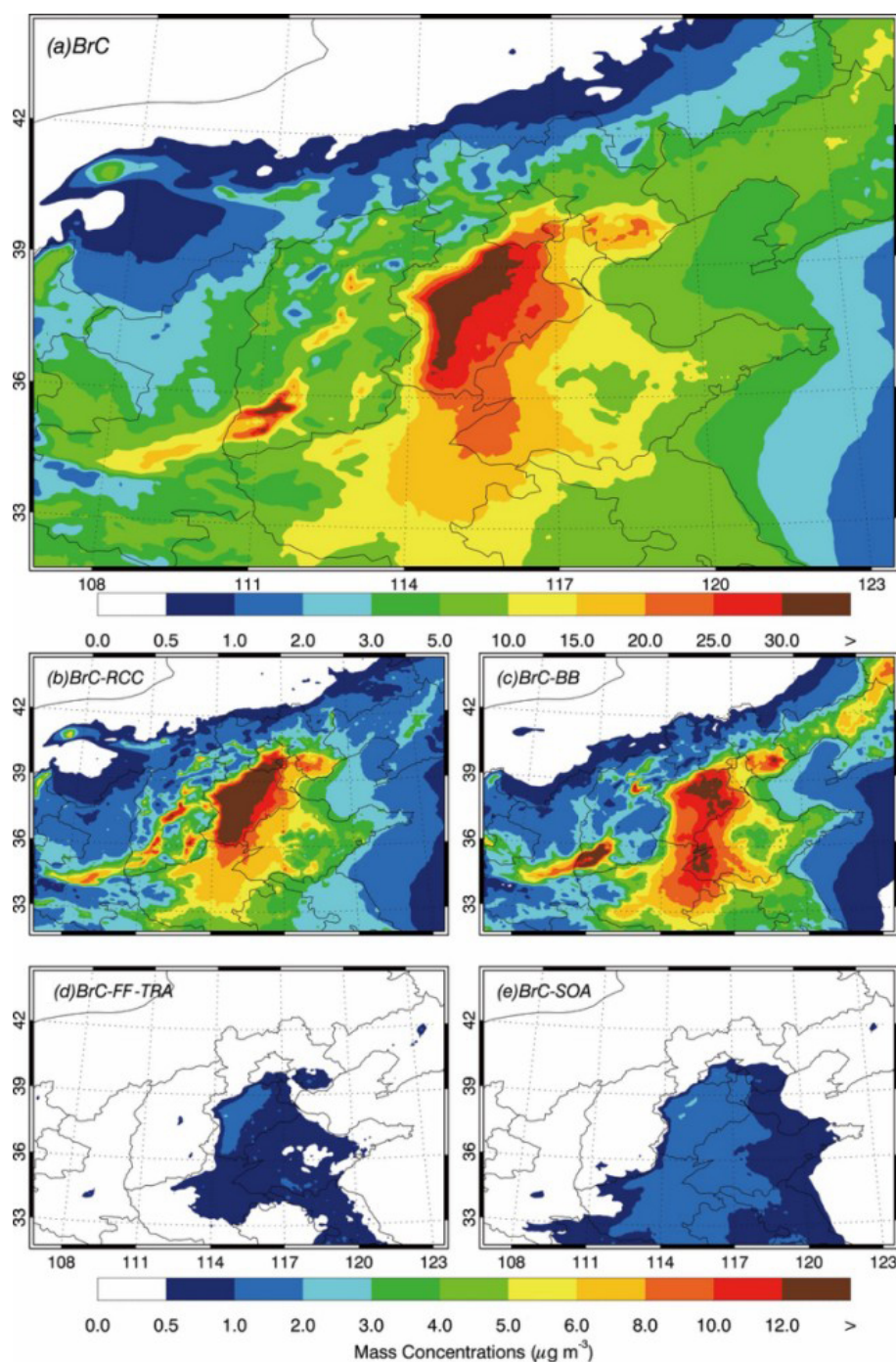
Figure 6. Simulated mean surface concentrations of BrC **(a)** and contributions from RCC **(b)**, BB **(c)**, FF-TRA **(d)** and secondary BrC **(e)** in January 2014 in the NCP.

They are higher than the surface ratio used in the global models (Jo et al., 2016; Park et al., 2010) but lower than the ratio of Feng et al. (2013). Although the concentration of BrC is relatively high and the absorption of BrC in the ultraviolet band is comparable to that of BC, the imaginary index of BrC (about 0.1) is still much lower than that of BC (about

0.76). As a result, the light absorption contribution of BrC at 365 nm is not as significant during the study period.

Furthermore, the light absorption properties of BrC during the winter season are predominantly attributed to RCC, followed by BB, SOA and FF-TRA in the NCP. The average contribution of RCC and BB to the AAOD of BrC is 59.3 % and 26.3 %, respectively. Although the concentra-
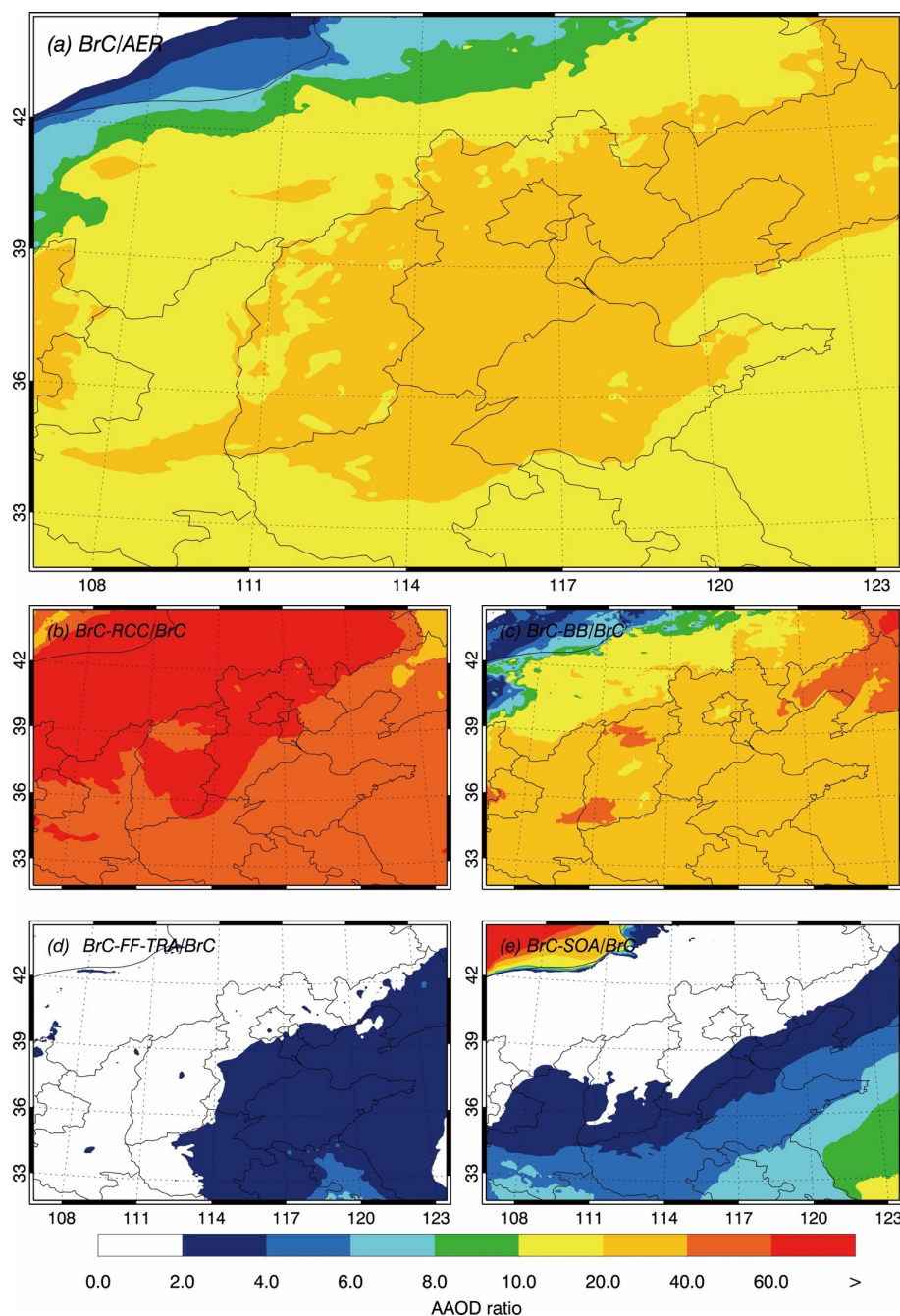
Figure 7. Simulated monthly BrC AAOD versus aerosol at 365 nm (**a**) and each anthropogenic source of RCC (**b**), BB (**c**), FF-TRA (**d**) and secondary BrC (**e**) AAOD versus BrC in the NCP.

tion of BrC from RCC is comparable to that from BB, the much higher light-absorbing property of the BrC from RCC makes it a dominant contributor to the overall light absorption caused by BrC. Despite lower surface concentrations compared to primary BrC, secondary BrC contributes significantly to AAOD of BrC, averaging $\sim 10.0\%$ with elevated contributions in the sea and remote regions, which is likely due to the highly oxidized character of organic

aerosols and its chemical aging in aging air masses, leading to the formation of BrC (Gouw et al., 2005; Kawamura et al., 2005; Tsigaridis and Kanakidou, 2018). While AOD represents column-integrated concentrations, the ratio of secondary BrC to primary BrC increases from 8.9 % at the surface to 12.0 % of atmospheric burden. It reaches 14.3 % at an altitude of 500 m as shown in Fig. S6, which could lead to a higher absorption contribution of secondary BrC (Wang et
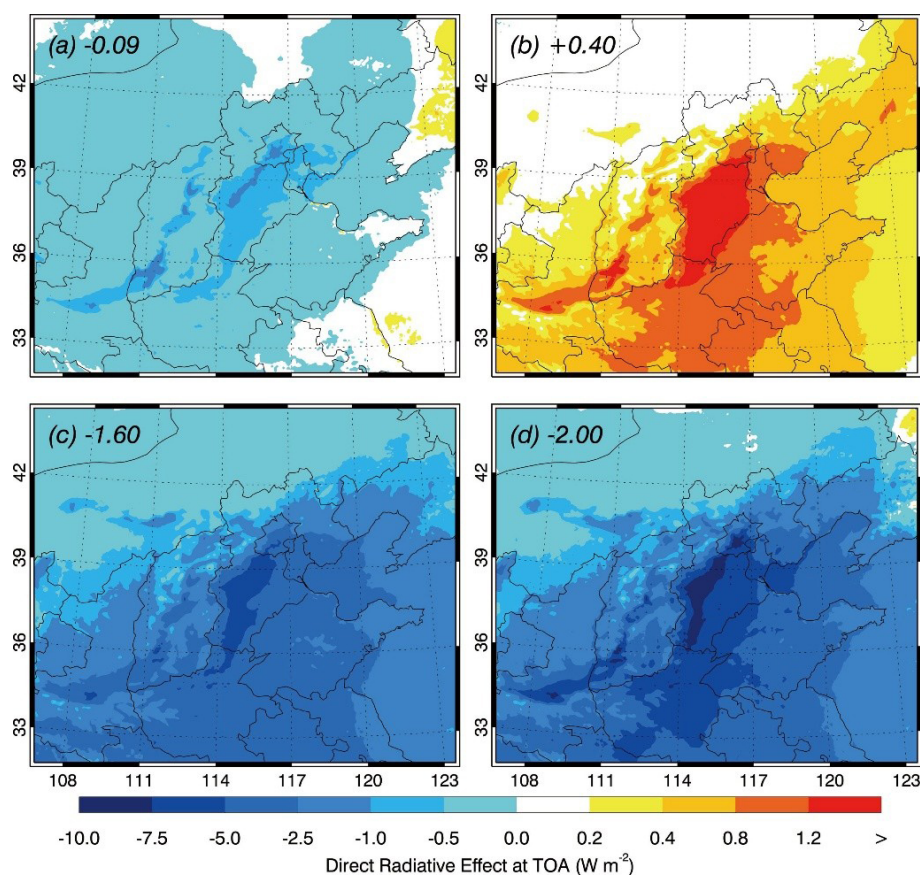
Figure 8. Estimated DRE_{TOA} of BrC **(a)** and DRE_{TOA} increase of OA owing to the absorption of BrC **(b)**. The DRE_{TOA} of total OA with absorbing BrC **(c)** and DRE_{TOA} of total OA with BrC is assumed to be scattering **(d)**. The averages of DRE are shown in the upper left of each panel.

al., 2022b). Moreover, the observations indicate that a substantial amount of SOA is water-soluble (Maria et al., 2003; Peng et al., 2021) and therefore treated as hygroscopic components in the model, and its absorption could be magnified. The AAOD contribution of BrC from vehicles is the lowest, about 1.8 % on average, but its contribution in southern Jiangsu and southeast Anhui ranges from 4 % to 8 %, higher than in other regions. This may suggest that motor vehicle emissions account for a significant proportion of pollution in this area.

3.4 Direct radiative effect of BrC

Figure 8a shows the distribution of the average DRE_{TOA} caused by BrC at the top of the atmosphere during the episode. The DRE_{TOA} of BrC in the NCP is $-0.09\,\mathrm{W\,m^{-2}}$ on average, with a maximum of $+0.46\,\mathrm{W\,m^{-2}}$ and a minimum of $-2.74\,\mathrm{W\,m^{-2}}$. Compared to the average DRE_{TOA} of BC $+3.9\,\mathrm{W\,m^{-2}}$ and a maximum of $+21.6\,\mathrm{W\,m^{-2}}$, the average DRE_{TOA} of BrC in the NCP is close to zero. However, in terms of the spatial distribution, the DRE_{TOA} of total BrC in the NCP is predominantly negative, especially

in those areas with high BrC concentrations including the BTH area and Fen-Wei Plain. The largest negative DRE_{TOA} is in Shanxi Province, where the highest contributor to BrC is BB. The overall scattering effect of BrC is greater than its absorption effect, so BrC has a net cooling effect. The solar irradiance in the UV band contributes only 10 % of the total solar irradiation, and the imaginary refractive indices of BrC are much lower than those strongly absorbing BC, especially in the visible band. On the other hand, although this leads to a small heating effect by BrC, the increased DRE_{TOA} induced by BrC, which is usually considered its scattering effect, is up to an average of $+0.40\,\mathrm{W\,m^{-2}}$ and a maximum of $+1.83\,\mathrm{W\,m^{-2}}$ as shown in Fig. 8b. The DRE_{TOA} of OA without BrC is $-2.00\,\mathrm{W\,m^{-2}}$ over the NCP (Fig. 8d) and is increased to $-1.60\,\mathrm{W\,m^{-2}}$ (Fig. 8c) after considering BrC. Consequently, the cooling effect of OA is reduced by BrC by an average of 28.0 %. So far, almost all estimates of the radiation effects of BrC are on a global basis. The study of Wang et al. (2014) reported a global DRE_{TOA} of BrC of $-0.02\,\mathrm{W\,m^{-2}}$, resulting in a DRE_{TOA} increase of $+0.07\,\mathrm{W\,m^{-2}}$. Brown et al. (2018) have also reported a global annual increased DRE_{TOA} of $+0.13\,\mathrm{W\,m^{-2}}$,
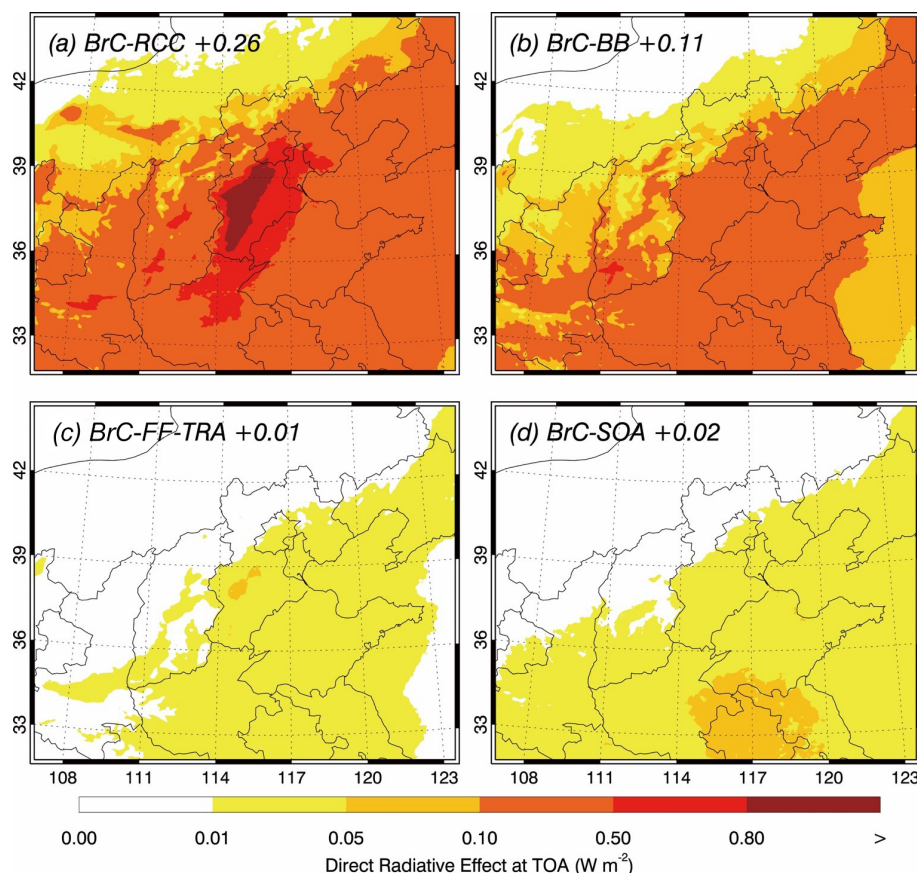
Figure 9. The estimation DRE_{TOA} of BrC from each anthropogenic source RCC **(a)**, BB **(b)**, FF-TRA **(c)** and secondary BrC **(d)** in the NCP in January 2014.

with the maximum forcing ($\sim +1.75\,\mathrm{W\,m^{-2}}$) occurring on the west coast of southern Africa. BrC reduces the cooling effect caused by organic aerosols by approximately 16 % (Jo et al., 2016). However, all these estimates only considered BB, biofuels or SOA and the significance of BrC in the estimates for these studies typically based on the assumption that OA primarily scatters sunlight. Our results indicate that the solar radiation changes caused by BrC in the NCP are notable. The absorption effect of BrC should be considered in climate models to accurately assess the aerosol impact on atmospheric heating and climate change.

Figure 9a–d show the estimated DRE_{TOA} of BrC from RCC, BB, FF-TRA and secondary BrC in the NCP during the episode. Similar to the contribution of BrC sources to the AAOD at 365 nm, the most important source contributing to DRE_{TOA} of BrC is RCC ($+0.26\,\mathrm{W\,m^{-2}}$), followed by BB ($+0.11\,\mathrm{W\,m^{-2}}$), secondary BrC ($+0.02\,\mathrm{W\,m^{-2}}$) and FF-TRA ($+0.01\,\mathrm{W\,m^{-2}}$) in the NCP, as shown in Fig. 9. In addition, the DRE_{TOA} of BrC from various sources exhibits distinct spatial distribution characteristics in the NCP. The highest DRE_{TOA} of BrC from fossil sources, which include RCC and FF-TRA, is predominantly concentrated in Hebei. The highest positive DRE_{TOA} of BrC from BB is found in the

Fen-Wei Plain. Meanwhile, the secondary BrC contributes most to the DRE_{TOA} in the south part of the NCP. The persistent high values over southern China might stem from the model's representation of secondary BrC as hygroscopic components (Peng et al., 2021), whose light-absorbing capacity is amplified in the region with high ambient humidity.

4 Conclusions

A source-explicit BrC simulation in January 2014 in the NCP is conducted by using the WRF-Chem model. We define the BrC based on varying proportions of RCC, BB, FF-TRA and SOA sources, assigning each a distinct imaginary refractive index to represent their differing light absorption characteristics. Model simulations are evaluated with various data sets. Besides the good reproduction of temporal and spatial variations of aerosol components and SWDOWN in the model, AOD and SSA are used to evaluate the aerosol optical properties.

Near-surface mass concentrations of simulated BrC in the NCP range from 0.05 to $42.3\,\mathrm{\mu g\,m^{-3}}$ with an average of $5.2\,\mathrm{\mu g\,m^{-3}}$, which is mainly attributed to RCC and BB, especially in the BTH region and Fen-Wei Plain. Estimation of

the BrC contribution to AAOD shows that the BrC accounts for an average of 16.4 % and up to 39.5 % of the total aerosol absorption at 365 nm. The largest contributor to the absorption of BrC is RCC-derived BrC, reaching 59.3 %. BrC generally has a net cooling effect in the NCP if we consider both the absorption and scattering properties, with DRE_{TOA} of BrC of around $-0.09\,\mathrm{W\,m^{-2}}$ on average and ranging between -2.74 and $+0.46\,\mathrm{W\,m^{-2}}$. However, the absorption of BrC increases the DRE_{TOA} of OA by 28.0 % with an average of $+0.40\,\mathrm{W\,m^{-2}}$ and a maximum of $+1.83\,\mathrm{W\,m^{-2}}$. The average increase in DRE_{TOA} of BrC from RCC, BB, secondary formation and FF-TRA is $+0.26$, $+0.11$, $+0.02$ and $+0.01\,\mathrm{W\,m^{-2}}$, respectively. Our results indicate that BrC derived from RCC may have significant implications for regions relying heavily on coal as their primary energy source, such as northern China. Climate models should not only incorporate the absorption of BrC but also account for residential coal burning as a potentially important BrC emission source. Additionally, although we conducted simulations with a relatively conservative secondary BrC, the impact of secondary BrC on radiative processes should not be overlooked. More field observation and model experiments should be carried out in the future for better understanding of its role in atmospheric radiation balance.

It should be noted that China has started to switch from coal to cleaner and more efficient energy such as natural gas or liquid petroleum gas in recent years. According to the latest report of National Bureau of Statistics of China, the total coal consumption for residential use was 55.5 Gg in 2022 (https://data.stats.gov.cn, last access: 10 March 2025) with a 40.3 % decrease compared to 2014. Therefore, our diagnosis of the sources of BrC and their radiative effects is specifically targeted at the winter season in 2014. Moreover, future simulations should strengthen the parameterization for the evolution of BrC, such as bleaching or darkening processes.

The simulation of BrC in climate models is fraught with uncertainties due to its diverse sources which result in a wide range of optical properties. The absorption characteristics of BrC can change significantly as it undergoes atmospheric aging, impacting its radiative forcing estimates. Additionally, interactions of BrC with other atmospheric particles and its effects on cloud microphysics and albedo introduce further complexities in modeling its climate impact. These uncertainties necessitate enhanced observational data and better integration of BrC properties in climate models to improve the accuracy of climate predictions and assessments. Although the simulations have been evaluated with extensive aerosol mass and optical measurements, more field measurements and lab experiments are needed, especially for the inventory development of BrC, the vertical profiles from aircraft and physicochemical properties, which would be useful for further evaluating and improving model performance.

References

Andreae, M. O. and Gelencsér, A.: Black carbon or brown carbon? The nature of light-absorbing carbonaceous aerosols, Atmos. Chem. Phys., 6, 3131–3148, https://doi.org/10.5194/acp-6-3131-2006, 2006.

Bai, K., Li, K., Ma, M., Li, K., Li, Z., Guo, J., Chang, N.-B., Tan, Z., and Han, D.: LGHAP: the Long-term Gap-free High-resolution Air Pollutant concentration dataset, derived via tensor-flow-based multimodal data fusion, Earth Syst. Sci. Data, 14, 907–927, https://doi.org/10.5194/essd-14-907-2022, 2022 (data available at: https://doi.org/10.12041/geodata.1776940.ver1.db).

Bohren, C. F. and Huffman, D. R.: Absorption and Scattering of Light by Small Particles, Wiley, ISBN 9780471293408, https://doi.org/10.1002/9783527618156, 1998.

Bond, T. C.: Spectral dependence of visible light absorption by carbonaceous particles emitted from coal combustion, Geophys. Res. Lett., 28, 4075–4078, https://doi.org/10.1029/2001GL013652, 2001.

Bond, T. C., Doherty, S. J., Fahey, D. W., Forster, P. M., Berntsen, T., DeAngelo, B. J., Flanner, M. G., Ghan, S., Kärcher, B., Koch, D., Kinne, S., Kondo, Y., Quinn, P. K., Sarofim, M. C., Schultz, M. G., Schulz, M., Venkataraman, C., Zhang, H., Zhang, S., Bellouin, N., Guttikunda, S. K., Hopke, P. K., Jacobson, M. Z., Kaiser, J. W., Klimont, Z., Lohmann, U., Schwarz, J. P., Shindell, D., Storelvmo, T., Warren, S. G., and Zender, C. S.: Bounding the role of black carbon in the climate system: A scientific assessment, J. Geophys. Res., 118, 5380–5552, https://doi.org/10.1002/jgrd.50171, 2013.

Brown, H., Liu, X., Feng, Y., Jiang, Y., Wu, M., Lu, Z., Wu, C., Murphy, S., and Pokhrel, R.: Radiative effect and climate impacts of brown carbon with the Community Atmosphere Model (CAM5), Atmos. Chem. Phys., 18, 17745–17768, https://doi.org/10.5194/acp-18-17745-2018, 2018.

Browne, E. C., Zhang, X., Franklin, J. P., Ridley, K. J., Kirchstetter, T. W., Wilson, K. R., Cappa, C. D., and Kroll, J. H.: Effect of heterogeneous oxidative aging on light absorption by biomass burning organic aerosol, Aerosol Sci. Tech., 53, 663–674, https://doi.org/10.1080/02786826.2019.1599321, 2019.

Cao, J. J. and Cui, L.: Current Status, Characteristics and Causes of Particulate Air Pollution in the Fenwei Plain, China: A Review, J. Geophys. Res., 126, e2020JD034472, https://doi.org/10.1029/2020JD034472, 2021.

Chakrabarty, R. K., Moosmüller, H., Chen, L.-W. A., Lewis, K., Arnott, W. P., Mazzoleni, C., Dubey, M. K., Wold, C. E., Hao, W. M., and Kreidenweis, S. M.: Brown carbon in tar balls from smoldering biomass combustion, Atmos. Chem. Phys., 10, 6363–6370, https://doi.org/10.5194/acp-10-6363-2010, 2010.

Chand, D., Wood, R., Ghan, S. J., Wang, M., Ovchinnikov, M., Rasch, P. J., Miller, S., Schichtel, B., and Moore, T.: Aerosol optical depth increase in partly cloudy conditions, J. Geophys. Res., 117, D17207, https://doi.org/10.1029/2012JD017894, 2012.

Chen, W., Wang, Z., Zhao, H., and Qin, K.: A novel way to calculate shortwave black carbon direct radiative effect, Sci. Total. Environ., 756, 142961, https://doi.org/10.1016/j.scitotenv.2020.142961, 2021.

Chen, Y. and Bond, T. C.: Light absorption by organic carbon from wood combustion, Atmos. Chem. Phys., 10, 1773–1787, https://doi.org/10.5194/acp-10-1773-2010, 2010.

Cheng, Z., Atwi, K. M., Yu, Z., Avery, A., Fortner, E. C., Williams, L., Majluf, F., Krechmer, J. E., Lambe, A. T., and Saleh, R.: Evolution of the light-absorption properties of combustion brown carbon aerosols following reaction with nitrate radicals, Aerosol Sci. Tech., 54, 849–863, https://doi.org/10.1080/02786826.2020.1726867, 2020.

China Environmental Monitoring Centre: National Urban Air Quality Real-time Release Platform, China Environmental Monitoring Center [data set], https://air.cnemc.cn:18007/, last access: 30 January 2014.

Corbin, J. C., Czech, H., Massabò, D., Mongeot, F. B. de, Jakobi, G., Liu, F., Lobo, P., Mennucci, C., Mensah, A. A., Orasche, J., Pieber, S. M., Prévôt, A. S. H., Stengel, B., Tay, L.-L., Zanatta, M., Zimmermann, R., El Haddad, I., and Gysel, M.: Infrared-absorbing carbonaceous tar can dominate light absorption by marine-engine exhaust, npj Clim. Atmos. Sci., 2, 3985, https://doi.org/10.1038/s41612-019-0069-5, 2019.

D'Almeida, G. A., Koepke, P., and Shettle, E. P.: Atmospheric Aerosols: Global Climatology and Radiative Characteristics, A, Deepak Publ., Hampton, Virginia, ISBN 0937194220, 1991.

Dubovik, O., Holben, B., Eck, T. F., Smirnov, A., Kaufman, Y. J., King, M. D., Tanré, D., and Slutsker, I.: Variability of Absorption and Optical Properties of Key Aerosol Types Observed in Worldwide Locations, J. Atmos. Sci., 59, 590–608, https://doi.org/10.1175/1520-0469(2002)059<0590:VOAAOP>2.0.CO;2, 2002.

Fast, J. D., Gustafson, W. I., Easter, R. C., Zaveri, R. A., Barnard, J. C., Chapman, E. G., Grell, G. A., and Peckham, S. E.: Evolution of ozone, particulates, and aerosol direct radiative forcing in the vicinity of Houston using a fully coupled meteorology-chemistry-aerosol model, J. Geophys. Res., 111, 2981, https://doi.org/10.1029/2005JD006721, 2006.

Feng, Y., Ramanathan, V., and Kotamarthi, V. R.: Brown carbon: a significant atmospheric absorber of solar radiation?, Atmos. Chem. Phys., 13, 8607–8621, https://doi.org/10.5194/acp-13-8607-2013, 2013.

Forrister, H., Liu, J., Scheuer, E., Dibb, J., Ziemba, L., Thornhill, K. L., Anderson, B., Diskin, G., Perring, A. E., Schwarz, J. P., Campuzano-Jost, P., Day, D. A., Palm, B. B., Jimenez, J. L., Nenes, A., and Weber, R. J.: Evolution of brown carbon in wildfire plumes, Geophys. Res. Lett., 42, 4623–4630, https://doi.org/10.1002/2015GL063897, 2015.

Fountoukis, C. and Nenes, A.: ISORROPIA II: a computationally efficient thermodynamic equilibrium model for $K^+-Ca^{2+}-Mg^{2+}-NH_4^+-Na^+-SO_4^{2-}-NO_3^--Cl^--H_2O$ aerosols, Atmos. Chem. Phys., 7, 4639–4659, https://doi.org/10.5194/acp-7-4639-2007, 2007.

Gao, Y., Gao, P., Zhuang, B., Hu, Y., Zhou, Y., Wang, T., Li, S., Li, M., and Xie, M.: Changes in the Climate Effects of Major Anthropogenic Aerosols in East Asia Under Different Emission Reduction Scenarios in China, J. Geophys. Res., 130, e2024JD042301, https://doi.org/10.1029/2024JD042301, 2025.

Ge, W., Prime, N. S., Smith, S. J., Liu, J., Ren, Y., Zhou, Y., Wu, H., Wang, X., and Chen, G.: The short-term comprehensive impact of the phase-out of global coal combustion on air pollution and climate change, Environ. Pollut., 367, 125669, https://doi.org/10.1016/j.envpol.2025.125669, 2025.

Gouw, J. A. de, Middlebrook, A. M., Warneke, C., Goldan, P. D., Kuster, W. C., Roberts, J. M., Fehsenfeld, F. C., Worsnop,

D. R., Canagaratna, M. R., Pszenny, A. A. P., Keene, W. C., Marchewka, M., Bertman, S. B., and Bates, T. S.: Budget of organic carbon in a polluted atmosphere: Results from the New England Air Quality Study in 2002, J. Geophys. Res., 110, D16305, https://doi.org/10.1029/2004JD005623, 2005.

Grell, G. A., Peckham, S. E., Schmitz, R., McKeen, S. A., Frost, G., Skamarock, W. C., and Eder, B.: Fully coupled "online" chemistry within the WRF model, Atmos. Environ., 39, 6957–6975, https://doi.org/10.1016/j.atmosenv.2005.04.027, 2005.

Guenther, A., Karl, T., Harley, P., Wiedinmyer, C., Palmer, P. I., and Geron, C.: Estimates of global terrestrial isoprene emissions using MEGAN (Model of Emissions of Gases and Aerosols from Nature), Atmos. Chem. Phys., 6, 3181–3210, https://doi.org/10.5194/acp-6-3181-2006, 2006.

Hammer, M. S., Martin, R. V., van Donkelaar, A., Buchard, V., Torres, O., Ridley, D. A., and Spurr, R. J. D.: Interpreting the ultraviolet aerosol index observed with the OMI satellite instrument to understand absorption by organic aerosols: implications for atmospheric oxidation and direct radiative effects, Atmos. Chem. Phys., 16, 2507–2523, https://doi.org/10.5194/acp-16-2507-2016, 2016.

Hecobian, A., Zhang, X., Zheng, M., Frank, N., Edgerton, E. S., and Weber, R. J.: Water-Soluble Organic Aerosol material and the light-absorption characteristics of aqueous extracts measured over the Southeastern United States, Atmos. Chem. Phys., 10, 5965–5977, https://doi.org/10.5194/acp-10-5965-2010, 2010.

Hoffer, A., Gelencsér, A., Guyon, P., Kiss, G., Schmid, O., Frank, G. P., Artaxo, P., and Andreae, M. O.: Optical properties of humic-like substances (HULIS) in biomass-burning aerosols, Atmos. Chem. Phys., 6, 3563–3570, https://doi.org/10.5194/acp-6-3563-2006, 2006.

Huang, R.-J., Yuan, W., Yang, L., Yang, H., Cao, W., Guo, J., Zhang, N., Zhu, C., Wu, Y., and Zhang, R.: Concentration, optical characteristics, and emission factors of brown carbon emitted by on-road vehicles, Sci. Total. Environ., 810, 151307, https://doi.org/10.1016/j.scitotenv.2021.151307, 2022.

Huang, X., Song, Y., Zhao, C., Cai, X., Zhang, H., and Zhu, T.: Direct Radiative Effect by Multicomponent Aerosol over China, J. Climate, 28, 3472–3495, https://doi.org/10.1175/JCLI-D-14-00365.1, 2015.

Hurley, M. D., Sokolov, O., Wallington, T. J., Takekawa, H., Karasawa, M., Klotz, B., Barnes, I., and Becker, K. H.: Organic aerosol formation during the atmospheric degradation of toluene, Environ. Sci. Technol., 35, 1358–1366, https://doi.org/10.1021/es0013733, 2001.

IPCC (Ed.): Climate Change 2013: The Physical Science Basis. Contribution of Working Group I to the Fifth Assessment Report of the Intergovernmental Panel on Climate Change, Cambridge University Press, Cambridge, United Kingdom and New York, NY, USA, ISBN 978-1-107-66182-0, https://www.ipcc.ch/report/ar5/wg1/ (last access: 12 July 2025), 2013.

Jacobson, M. Z.: Isolating nitrated and aromatic aerosols and nitrated aromatic gases as sources of ultraviolet light absorption, J. Geophys. Res., 104, 3527–3542, https://doi.org/10.1029/1998JD100054, 1999.

Jacobson, M. Z.: Effects of biomass burning on climate, accounting for heat and moisture fluxes, black and brown carbon, and cloud absorption effects, J. Geophys. Res., 119, 8980–9002, https://doi.org/10.1002/2014JD021861, 2014.

Jeong, J. I., Jo, D. S., Park, R. J., Lee, H.-M., Curci, G., and Kim, S.-W.: Parametric analysis for global single scattering albedo calculations, Atmos. Environ., 234, 117616, https://doi.org/10.1016/j.atmosenv.2020.117616, 2020.

Jo, D. S., Park, R. J., Lee, S., Kim, S.-W., and Zhang, X.: A global simulation of brown carbon: implications for photochemistry and direct radiative effect, Atmos. Chem. Phys., 16, 3413–3432, https://doi.org/10.5194/acp-16-3413-2016, 2016.

Jo, D. S., Nault, B. A., Tilmes, S., Gettelman, A., McCluskey, C. S., Hodzic, A., Henze, D. K., Nawaz, M. O., Fung, K. M., and Jimenez, J. L.: Global Health and Climate Effects of Organic Aerosols from Different Sources, Environ. Sci. Technol., 57, 13793–13807, https://doi.org/10.1021/acs.est.3c02823, 2023.

Kawamura, K., Imai, Y., and Barrie, L. A.: Photochemical production and loss of organic acids in high Arctic aerosols during long-range transport and polar sunrise ozone depletion events, Atmos. Environ., 39, 599–614, https://doi.org/10.1016/j.atmosenv.2004.10.020, 2005.

Kirchstetter, T. W., Novakov, T., and Hobbs, P. V.: Evidence that the spectral dependence of light absorption by aerosols is affected by organic carbon, J. Geophys. Res., 109, D21208, https://doi.org/10.1029/2004JD004999, 2004.

Kumar, N. K., Corbin, J. C., Bruns, E. A., Massabó, D., Slowik, J. G., Drinovec, L., Močnik, G., Prati, P., Vlachou, A., Baltensperger, U., Gysel, M., El-Haddad, I., and Prévôt, A. S. H.: Production of particulate brown carbon during atmospheric aging of residential wood-burning emissions, Atmos. Chem. Phys., 18, 17843–17861, https://doi.org/10.5194/acp-18-17843-2018, 2018.

Lack, D. A., Langridge, J. M., Bahreini, R., Cappa, C. D., Middlebrook, A. M., and Schwarz, J. P.: Brown carbon and internal mixing in biomass burning particles, P. Natl. Acad. Sci. USA, 109, 14802–14807, https://doi.org/10.1073/pnas.1206575109, 2012.

Laskin, A., Laskin, J., and Nizkorodov, S. A.: Chemistry of atmospheric brown carbon, Chem. Rev., 115, 4335–4382, https://doi.org/10.1021/cr5006167, 2015.

Li, C., He, Q., Hettiyadura, A. P. S., Käfer, U., Shmul, G., Meidan, D., Zimmermann, R., Brown, S. S., George, C., Laskin, A., and Rudich, Y.: Formation of Secondary Brown Carbon in Biomass Burning Aerosol Proxies through NO_3 Radical Reactions, Environ. Sci. Technol., 54, 1395–1405, https://doi.org/10.1021/acs.est.9b05641, 2020.

Li, G., Lei, W., Zavala, M., Volkamer, R., Dusanter, S., Stevens, P., and Molina, L. T.: Impacts of HONO sources on the photochemistry in Mexico City during the MCMA-2006/MILAGO Campaign, Atmos. Chem. Phys., 10, 6551–6567, https://doi.org/10.5194/acp-10-6551-2010, 2010.

Li, G., Bei, N., Tie, X., and Molina, L. T.: Aerosol effects on the photochemistry in Mexico City during MCMA-2006/MILAGRO campaign, Atmos. Chem. Phys., 11, 5169–5182, https://doi.org/10.5194/acp-11-5169-2011, 2011a.

Li, G., Zavala, M., Lei, W., Tsimpidi, A. P., Karydis, V. A., Pandis, S. N., Canagaratna, M. R., and Molina, L. T.: Simulations of organic aerosol concentrations in Mexico City using the WRF-CHEM model during the MCMA-2006/MILAGRO campaign, Atmos. Chem. Phys., 11, 3789–3809, https://doi.org/10.5194/acp-11-3789-2011, 2011b.

Li, G., Lei, W., Bei, N., and Molina, L. T.: Contribution of garbage burning to chloride and $PM_{2.5}$ in Mexico City, At-

mos. Chem. Phys., 12, 8751–8761, https://doi.org/10.5194/acp-12-8751-2012, 2012.

Li, M., Liu, H., Geng, G., Hong, C., Liu, F., Song, Y., Tong, D., Zheng, B., Cui, H., Man, H., Zhang, Q., and He, K.: Anthropogenic emission inventories in China: a review, Natl. Sci. Rev., 4, 834–866, https://doi.org/10.1093/nsr/nwx150, 2017.

Li, M., Fan, X., Zhu, M., Zou, C., Song, J., Wei, S., Jia, W., and Peng, P.'a.: Abundance and Light Absorption Properties of Brown Carbon Emitted from Residential Coal Combustion in China, Environ. Sci. Technol., 53, 595–603, https://doi.org/10.1021/acs.est.8b05630, 2019.

Li, X., Wu, J., Elser, M., Feng, T., Cao, J., El-Haddad, I., Huang, R., Tie, X., Prévôt, A. S. H., and Li, G.: Contributions of residential coal combustion to the air quality in Beijing–Tianjin–Hebei (BTH), China: a case study, Atmos. Chem. Phys., 18, 10675–10691, https://doi.org/10.5194/acp-18-10675-2018, 2018.

Lin, G., Penner, J. E., Flanner, M. G., Sillman, S., Xu, L., and Zhou, C.: Radiative forcing of organic aerosol in the atmosphere and on snow: Effects of SOA and brown carbon, J. Geophys. Res., 119, 7453–7476, https://doi.org/10.1002/2013JD021186, 2014.

Lin, P., Bluvshtein, N., Rudich, Y., Nizkorodov, S. A., Laskin, J., and Laskin, A.: Molecular Chemistry of Atmospheric Brown Carbon Inferred from a Nationwide Biomass Burning Event, Environ. Sci. Technol., 51, 11561–11570, https://doi.org/10.1021/acs.est.7b02276, 2017.

Liu, D., Whitehead, J., Alfarra, M. R., Reyes-Villegas, E., Spracklen, D. V., Reddington, C. L., Kong, S., Williams, P. I., Ting, Y.-C., Haslett, S., Taylor, J. W., Flynn, M. J., Morgan, W. T., McFiggans, G., Coe, H., and Allan, J. D.: Black-carbon absorption enhancement in the atmosphere determined by particle mixing state, Nat. Geosci., 10, 184–188, https://doi.org/10.1038/ngeo2901, 2017.

Liu, J., Bergin, M., Guo, H., King, L., Kotra, N., Edgerton, E., and Weber, R. J.: Size-resolved measurements of brown carbon in water and methanol extracts and estimates of their contribution to ambient fine-particle light absorption, Atmos. Chem. Phys., 13, 12389–12404, https://doi.org/10.5194/acp-13-12389-2013, 2013.

Lu, Z., Streets, D. G., Winijkul, E., Yan, F., Chen, Y., Bond, T. C., Feng, Y., Dubey, M. K., Liu, S., Pinto, J. P., and Carmichael, G. R.: Light absorption properties and radiative effects of primary organic aerosol emissions, Environ. Sci. Technol., 49, 4868–4877, https://doi.org/10.1021/acs.est.5b00211, 2015.

Ma, Y., Jin, Y., Zhang, M., Gong, W., Hong, J., Jin, S., Shi, Y., Zhang, Y., and Liu, B.: Aerosol optical properties of haze episodes in eastern China based on remote-sensing observations and WRF-Chem simulations, Sci. Total. Environ., 757, 143784, https://doi.org/10.1016/j.scitotenv.2020.143784, 2021.

Maria, S. F., Russell, L. M., Turpin, B. J., Porcja, R. J., Campos, T. L., Weber, R. J., and Huebert, B. J.: Source signatures of carbon monoxide and organic functional groups in Asian Pacific Regional Aerosol Characterization Experiment (ACE-Asia) submicron aerosol types, J. Geophys. Res., 108, 295, https://doi.org/10.1029/2003JD003703, 2003.

Mo, Y., Li, J., Cheng, Z., Zhong, G., Zhu, S., Tian, C., Chen, Y., and Zhang, G.: Dual Carbon Isotope-Based Source Apportionment and Light Absorption Properties of Water-Soluble Organic Carbon in $PM_{2.5}$ Over China, J. Geophys. Res., 126, 27805, https://doi.org/10.1029/2020JD033920, 2021.

Moise, T., Flores, J. M., and Rudich, Y.: Optical properties of secondary organic aerosols and their changes by chemical processes, Chem. Rev., 115, 4400–4439, https://doi.org/10.1021/cr5005259, 2015.

Mukai, H. and Ambe, Y.: Characterization of a humic acid-like brown substance in airborne particulate matter and tentative identification of its origin, Atmos. Environ., 20, 813–819, https://doi.org/10.1016/0004-6981(86)90265-9, 1986.

Nenes, A., Pandis, S. N., and Christodoulos, P.: ISORROPIA: A New Thermodynamic Equilibrium Model for Multiphase Multicomponent Inorganic Aerosols, Aquat. Geochem., 4, 123–152, 1998.

Ni, H., Huang, R.-j., Pieber, S. M., Corbin, J. C., Stefenelli, G., Pospisilova, V., Klein, F., Gysel-Beer, M., Yang, L., Baltensperger, U., Haddad, I. E., Slowik, J. G., Cao, J., Prévôt, A. S. H., and Dusek, U.: Brown Carbon in Primary and Aged Coal Combustion Emission, Environ. Sci. Technol., 55, 5701–5710, https://doi.org/10.1021/acs.est.0c08084, 2021.

Park, R. J., Kim, M. J., Jeong, J. I., Youn, D., and Kim, S.: A contribution of brown carbon aerosol to the aerosol light absorption and its radiative forcing in East Asia, Atmos. Environ., 44, 1414–1421, https://doi.org/10.1016/j.atmosenv.2010.01.042, 2010.

Peng, C., Razafindrambinina, P. N., Malek, K. A., Chen, L., Wang, W., Huang, R.-J., Zhang, Y., Ding, X., Ge, M., Wang, X., Asa-Awuku, A. A., and Tang, M.: Interactions of organosulfates with water vapor under sub- and supersaturated conditions, Atmos. Chem. Phys., 21, 7135–7148, https://doi.org/10.5194/acp-21-7135-2021, 2021.

Pokhrel, R. P., Beamesderfer, E. R., Wagner, N. L., Langridge, J. M., Lack, D. A., Jayarathne, T., Stone, E. A., Stockwell, C. E., Yokelson, R. J., and Murphy, S. M.: Relative importance of black carbon, brown carbon, and absorption enhancement from clear coatings in biomass burning emissions, Atmos. Chem. Phys., 17, 5063–5078, https://doi.org/10.5194/acp-17-5063-2017, 2017.

Saleh, R.: From Measurements to Models: Toward Accurate Representation of Brown Carbon in Climate Calculations, Curr. Pollution Rep., 6, 90–104, https://doi.org/10.1007/s40726-020-00139-3, 2020.

Saleh, R., Robinson, E. S., Tkacik, D. S., Ahern, A. T., Liu, S., Aiken, A. C., Sullivan, R. C., Presto, A. A., Dubey, M. K., Yokelson, R. J., Donahue, N. M., and Robinson, A. L.: Brownness of organics in aerosols from biomass burning linked to their black carbon content, Nat. Geosci., 7, 647–650, https://doi.org/10.1038/ngeo2220, 2014.

Saleh, R., Cheng, Z., and Atwi, K.: The Brown–Black Continuum of Light-Absorbing Combustion Aerosols, Environ. Sci. Tech. Let., 5, 508–513, https://doi.org/10.1021/acs.estlett.8b00305, 2018.

Satheesh, S. K., Vinoj, V., and Krishnamoorthy, K.: Assessment of Aerosol Radiative Impact over Oceanic Regions Adjacent to Indian Subcontinent Using Multisatellite Analysis, Adv. Meteorol., 2010, 130, https://doi.org/10.1155/2010/139186, 2010.

Sengupta, D., Samburova, V., Bhattarai, C., Kirillova, E., Mazzoleni, L., Iaukea-Lum, M., Watts, A., Moosmüller, H., and Khlystov, A.: Light absorption by polar and non-polar aerosol compounds from laboratory biomass combustion, Atmos. Chem. Phys., 18, 10849–10867, https://doi.org/10.5194/acp-18-10849-2018, 2018.

Shapiro, E. L., Szprengiel, J., Sareen, N., Jen, C. N., Giordano, M. R., and McNeill, V. F.: Light-absorbing secondary organic material formed by glyoxal in aqueous aerosol mimics, Atmos. Chem. Phys., 9, 2289–2300, https://doi.org/10.5194/acp-9-2289-2009, 2009.

Song, S., Wang, Y., Wang, Y., Wang, T., and Tan, H.: The characteristics of particulate matter and optical properties of Brown carbon in air lean condition related to residential coal combustion, Powder Technol., 379, 505–514, https://doi.org/10.1016/j.powtec.2020.10.082, 2021.

Stein-Zweers, D. and Veefkind, P.: OMI/Aura Multi-wavelength Aerosol Optical Depth and Single Scattering Albedo L3 1 day Best Pixel in 0.25 degree x 0.25 degree V3, NASA Goddard Space Flight Center, Goddard Earth Sciences Data and Information Services Center (GES DISC) [data set], https://doi.org/10.5067/Aura/OMI/DATA3004, 2012.

Stokes, R. H. and Robinson, R. A.: Interactions in Aqueous Nonelectrolyte Solutions. I. Solute-Solvent Equilibria, J. Phys. Chem., 70, 2126–2131, https://doi.org/10.1021/j100879a010, 1966.

Sun, J., Zhi, G., Hitzenberger, R., Chen, Y., Tian, C., Zhang, Y., Feng, Y., Cheng, M., Zhang, Y., Cai, J., Chen, F., Qiu, Y., Jiang, Z., Li, J., Zhang, G., and Mo, Y.: Emission factors and light absorption properties of brown carbon from household coal combustion in China, Atmos. Chem. Phys., 17, 4769–4780, https://doi.org/10.5194/acp-17-4769-2017, 2017.

Sun, J., Zhang, Y., Zhi, G., Hitzenberger, R., Jin, W., Chen, Y., Wang, L., Tian, C., Li, Z., Chen, R., Xiao, W., Cheng, Y., Yang, W., Yao, L., Cao, Y., Huang, D., Qiu, Y., Xu, J., Xia, X., Yang, X., Zhang, X., Zong, Z., Song, Y., and Wu, C.: Brown carbon's emission factors and optical characteristics in household biomass burning: developing a novel algorithm for estimating the contribution of brown carbon, Atmos. Chem. Phys., 21, 2329–2341, https://doi.org/10.5194/acp-21-2329-2021, 2021.

Tang, J., Li, J., Su, T., Han, Y., Mo, Y., Jiang, H., Cui, M., Jiang, B., Chen, Y., Tang, J., Song, J., Peng, P., and Zhang, G.: Molecular compositions and optical properties of dissolved brown carbon in biomass burning, coal combustion, and vehicle emission aerosols illuminated by excitation–emission matrix spectroscopy and Fourier transform ion cyclotron resonance mass spectrometry analysis, Atmos. Chem. Phys., 20, 2513–2532, https://doi.org/10.5194/acp-20-2513-2020, 2020.

Tian, J., Wang, Q., Ni, H., Wang, M., Zhou, Y., Han, Y., Shen, Z., Pongpiachan, S., Zhang, N., Zhao, Z., Zhang, Q., Zhang, Y., Long, X., and Cao, J.: Emission Characteristics of Primary Brown Carbon Absorption From Biomass and Coal Burning: Development of an Optical Emission Inventory for China, J. Geophys. Res.-Atmos., 15, 27,805, https://doi.org/10.1029/2018JD029352, 2019.

Tsigaridis, K. and Kanakidou, M.: The Present and Future of Secondary Organic Aerosol Direct Forcing on Climate, Curr. Clim. Change Rep., 4, 84–98, https://doi.org/10.1007/s40641-018-0092-3, 2018.

Tuccella, P., Curci, G., Pitari, G., Lee, S., and Jo, D. S.: Direct Radiative Effect of Absorbing Aerosols: Sensitivity to Mixing State, Brown Carbon, and Soil Dust Refractive Index and Shape, J. Geophys. Res.-Atmos., 125, 317, https://doi.org/10.1029/2019JD030967, 2020.

Turpin, B. J. and Lim, H.-J.: Species Contributions to $PM_{2.5}$ Mass Concentrations: Revisiting Common Assumptions for Estimating Organic Mass, Aerosol Sci. Tech., 35, 602–610, https://doi.org/10.1080/02786820152051454, 2001.

Wang, J., Ye, J., Zhang, Q., Zhao, J., Wu, Y., Li, J., Liu, D., Li, W., Zhang, Y., Wu, C., Xie, C., Qin, Y., Lei, Y., Huang, X., Guo, J., Liu, P., Fu, P., Li, Y., Lee, H. C., Choi, H., Zhang, J., Liao, H., Chen, M., Sun, Y., Ge, X., Martin, S. T., and Jacob, D. J.: Aqueous production of secondary organic aerosol from fossil-fuel emissions in winter Beijing haze, P. Natl. Acad. Sci. USA, 118, https://doi.org/10.1073/pnas.2022179118, 2021.

Wang, Q., Zhou, Y., Ma, N., Zhu, Y., Zhao, X., Zhu, S., Tao, J., Hong, J., Wu, W., Cheng, Y., and Su, H.: Review of Brown Carbon Aerosols in China: Pollution Level, Optical Properties, and Emissions, J. Geophys. Res., 127, 455, https://doi.org/10.1029/2021JD035473, 2022a.

Wang, Q., Wang, L., Gong, C., Li, M., Xin, J., Tang, G., Sun, Y., Gao, J., Wang, Y., Wu, S., Kang, Y., Yang, Y., Li, T., Liu, J., and Wang, Y.: Vertical evolution of black and brown carbon during pollution events over North China Plain, Sci. Total. Environ., 806, 150950, https://doi.org/10.1016/j.scitotenv.2021.150950, 2022b.

Wang, X., Heald, C. L., Ridley, D. A., Schwarz, J. P., Spackman, J. R., Perring, A. E., Coe, H., Liu, D., and Clarke, A. D.: Exploiting simultaneous observational constraints on mass and absorption to estimate the global direct radiative forcing of black carbon and brown carbon, Atmos. Chem. Phys., 14, 10989–11010, https://doi.org/10.5194/acp-14-10989-2014, 2014.

Wang, X., Heald, C. L., Liu, J., Weber, R. J., Campuzano-Jost, P., Jimenez, J. L., Schwarz, J. P., and Perring, A. E.: Exploring the observational constraints on the simulation of brown carbon, Atmos. Chem. Phys., 18, 635–653, https://doi.org/10.5194/acp-18-635-2018, 2018.

Wang, Y., Wang, Y., Song, S., Wang, T., Li, D., and Tan, H.: Effects of coal types and combustion conditions on carbonaceous aerosols in flue gas and their light absorption properties, Fuel, 277, 118148, https://doi.org/10.1016/j.fuel.2020.118148, 2020.

Washenfelder, R. A., Attwood, A. R., Brock, C. A., Guo, H., Xu, L., Weber, R. J., Ng, N. L., Allen, H. M., Ayres, B. R., Baumann, K., Cohen, R. C., Draper, D. C., Duffey, K. C., Edgerton, E., Fry, J. L., Hu, W. W., Jimenez, J. L., Palm, B. B., Romer, P., Stone, E. A., Wooldridge, P. J., and Brown, S. S.: Biomass burning dominates brown carbon absorption in the rural southeastern United States, Geophys. Res. Lett., 42, 653–664, https://doi.org/10.1002/2014GL062444, 2015.

Wong, J. P. S., Tsagkaraki, M., Tsiodra, I., Mihalopoulos, N., Violaki, K., Kanakidou, M., Sciare, J., Nenes, A., and Weber, R. J.: Atmospheric evolution of molecular-weight-separated brown carbon from biomass burning, Atmos. Chem. Phys., 19, 7319–7334, https://doi.org/10.5194/acp-19-7319-2019, 2019.

Wu, J., Bei, N., Hu, B., Liu, S., Wang, Y., Shen, Z., Li, X., Liu, L., Wang, R., Liu, Z., Cao, J., Tie, X., Molina, L. T., and Li, G.: Aerosol-photolysis interaction reduces particulate matter during wintertime haze events, P. Natl. Acad. Sci. USA, 117, 9755–9761, https://doi.org/10.1073/pnas.1916775117, 2020.

Xie, C., Xu, W., Wang, J., Wang, Q., Liu, D., Tang, G., Chen, P., Du, W., Zhao, J., Zhang, Y., Zhou, W., Han, T., Bian, Q., Li, J., Fu, P., Wang, Z., Ge, X., Allan, J., Coe, H., and Sun, Y.: Vertical characterization of aerosol optical properties and brown carbon

in winter in urban Beijing, China, Atmos. Chem. Phys., 19, 165–179, https://doi.org/10.5194/acp-19-165-2019, 2019.

Xie, M., Hays, M. D., and Holder, A. L.: Light-absorbing organic carbon from prescribed and laboratory biomass burning and gasoline vehicle emissions, Scientific Reports, 7, 7318, https://doi.org/10.1038/s41598-017-06981-8, 2017.

Xu, L., Lin, G., Liu, X., Wu, C., Wu, Y., and Lou, S.: Constraining Light Absorption of Brown Carbon in China and Implications for Aerosol Direct Radiative Effect, Geophys. Res. Lett., 51, 455, https://doi.org/10.1029/2024GL109861, 2024.

Yan, C., Zheng, M., Bosch, C., Andersson, A., Desyaterik, Y., Sullivan, A. P., Collett, J. L., Zhao, B., Wang, S., He, K., and Gustafsson, Ö.: Important fossil source contribution to brown carbon in Beijing during winter, Scientific reports, 7, 43182, https://doi.org/10.1038/srep43182, 2017.

Yan, J., Wang, X., Gong, P., Wang, C., and Cong, Z.: Review of brown carbon aerosols: Recent progress and perspectives, Sci. Total. Environ., 634, 1475–1485, https://doi.org/10.1016/j.scitotenv.2018.04.083, 2018.

Yang, M., Howell, S. G., Zhuang, J., and Huebert, B. J.: Attribution of aerosol light absorption to black carbon, brown carbon, and dust in China – interpretations of atmospheric measurements during EAST-AIRE, Atmos. Chem. Phys., 9, 2035–2050, https://doi.org/10.5194/acp-9-2035-2009, 2009.

Zhang, A., Wang, Y., Zhang, Y., Weber, R. J., Song, Y., Ke, Z., and Zou, Y.: Modeling the global radiative effect of brown carbon: a potentially larger heating source in the tropical free troposphere than black carbon, Atmos. Chem. Phys., 20, 1901–1920, https://doi.org/10.5194/acp-20-1901-2020, 2020.

Zhang, Q., Streets, D. G., Carmichael, G. R., He, K. B., Huo, H., Kannari, A., Klimont, Z., Park, I. S., Reddy, S., Fu, J. S., Chen, D., Duan, L., Lei, Y., Wang, L. T., and Yao, Z. L.: Asian emissions in 2006 for the NASA INTEX-B mission, Atmos. Chem. Phys., 9, 5131–5153, https://doi.org/10.5194/acp-9-5131-2009, 2009.

Zhang, Q., Li, Z., Shen, Z., Zhang, T., Zhang, Y., Sun, J., Zeng, Y., Xu, H., Wang, Q., Hang Ho, S. S., and Cao, J.: Source profiles of molecular structure and light absorption of $PM_{2.5}$ brown carbon from residential coal combustion emission in Northwestern China, J. Environ. Sci. (China), 299, 118866, https://doi.org/10.1016/j.envpol.2022.118866, 2022a.

Zhang, W., Wang, W., Li, J., Ma, S., Lian, C., Li, K., Shi, B., Liu, M., Li, Y., Wang, Q., Sun, Y., Tong, S., and Ge, M.: Light absorption properties and potential sources of brown carbon in Fenwei Plain during winter 2018–2019, J. Environ. Sci., 102, 53–63, https://doi.org/10.1016/j.jes.2020.09.007, 2021.

Zhang, Y., Wang, Q., Tian, J., Li, Y., Liu, H., Ran, W., Han, Y., Prévôt, A. S.H., and Cao, J.: Impact of COVID-19 lockdown on the optical properties and radiative effects of urban brown carbon aerosol, Geosci. Front., 13, 101320, https://doi.org/10.1016/j.gsf.2021.101320, 2022b.

Zhao, C., Ruby Leung, L., Easter, R., Hand, J., and Avise, J.: Characterization of speciated aerosol direct radiative forcing over California, J. Geophys. Res., 118, 2372–2388, https://doi.org/10.1029/2012JD018364, 2013.

Zhu, Y., Wang, Q., Yang, X., Yang, N., and Wang, X.: Modeling Investigation of Brown Carbon Aerosol and Its Light Absorption in China, Atmosphere, 12, 892, https://doi.org/10.3390/atmos12070892, 2021.